CrystEngComm

Cite this: *CrystEngComm*, 2012, **14**, 6916–6920

www.rsc.org/crystengcomm

PAPER

Morphology-controlled synthesis of anisotropic wurtzite MnSe nanocrystals: optical and magnetic properties†

Xinyi Yang,[a] Yingnan Wang,[a] Yongming Sui,[a] Xiaoli Huang,[a] Tian Cui,[a] Chunzhong Wang,[b] Bingbing Liu,[a] Guangtian Zou[a] and Bo Zou*[a]

Received 11th May 2012, Accepted 16th July 2012
DOI: 10.1039/c2ce25741f

Manipulating the shape and size of metastable semiconductor nanocrystals (NCs) is important in various applications. In this work, anisotropic tetrapod- and waterdrop-shaped MnSe NCs with wurtzite (WZ) structure have been successfully synthesized by a one-pot solvothermal approach. The morphology, size and crystal structure have been investigated using transmission electron microscopy (TEM), high-resolution transmission electron microscopy (HRTEM) and powder X-ray diffraction (XRD). It was found that the shape and aspect ratio of WZ-MnSe NCs can be easily controlled by simply varying the heating rates. Furthermore, these WZ-MnSe NCs display blue–violet emission, which may find applications in full-colour display and short wavelength optoelectronic devices. The magnetic measurements indicate that the Néel temperature is found to be reduced with decreasing nanocrystal diameter. The size-dependent phase-transition behavior is attributed to the surface effect.

Introduction

Semiconductor nanocrystals (NCs) have attracted great interest in the areas of both fundamental research and technical application, because the chemical and physical properties of NCs depend strongly on their shape, size and crystal structure.[1–6] Manoeuvring the shape and size of the semiconductor NCs has long been considered as a powerful means for tailoring their properties and enhancing their performance in a wide variety of applications, including solar cells,[7] photodetectors,[8] electronic devices[9] and sensors.[10] In particular, current research has been focused on anisotropic shaped NCs such as nanotetrapods and nanorods since morphological anisotropy results in very complex physical properties and self-assembly behaviors compared to those of spherical nanoparticles.[11,12] Besides the shape and size, the crystal structure also can influence the optical/electrical properties of NCs.[13,14] For example, metastable NCs are expected to show unique optical and magnetic properties compared with the corresponding stable phase.[15,16] Therefore, simple methods are required to be developed in order to easily manipulate the nucleation and growth, and thus to tune the shape and size of metastable NCs.

Manganese chalcogenides exhibit a variety of important magneto-optical properties that result from their crystal structures.[17] Especially, manganese selenide (MnSe) is an antiferromagnetic semiconductor with interesting magnetic ordering, which can be tuned with dimensionality, thickness and strain in thin-film superlattices.[18,19] It can crystallize into three kinds of structural forms: the rock salt (RS), the zinc blend (ZB) and the wurtzite (WZ) structures. In contrast to many studies focusing on the synthesis and properties of stable RS-MnSe,[20,21] only a few reports can be found concerning metastable ZB- and WZ-MnSe.[22,23] In addition, these obtained ZB- and WZ-MnSe in previous works have been observed mainly as thin films or minor impurity phases. Because of their direct structural compatibility with III/V, II/VI and related semiconductor systems, metastable ZB- and WZ-MnSe are often found as a component in ternary semiconductor materials.[24] Because of the inability to obtain nominally phase-pure, bulk-scale quantities of the metastable MnSe (particularly the WZ structure), some detailed studies of their structures and properties are hampered. This represents a significant gap in this important family of magnetic semiconductors. Recently, Schaak *et al.* have succeeded in fabricating isotropic WZ-MnSe nanoparticles by a colloidal synthesis approach.[17] However, to the best of our knowledge, there have been no reports on the morphology-controlled synthesis of anisotropic WZ-MnSe NCs.

In this work, we report the synthesis of anisotropic tetrapod- and waterdrop-shaped WZ-MnSe NCs by a one-pot solvothermal method for the first time. Importantly, this work provides a facile strategy in the synthesis of shape-controlled MnSe NCs through simply tuning the heating rates. Blue-violet photoluminescence bands of the resulting NCs are observed while magnetic

[a]*State Key Laboratory of Superhard Materials, Jilin University, Changchun 130012, China. E-mail: zoubo@jlu.edu.cn*
[b]*Key Laboratory of Physics and Technology for Advanced Batteries (Ministry of Education), College of Physics, Jilin University, Changchun, 130012, China*
† Electronic supplementary information (ESI) available. See DOI: 10.1039/c2ce25741f

measurements indicate that Néel temperature is found to be reduced with decreasing nanocrystal diameter.

Experimental section

Chemical reagents

Anhydrous $MnCl_2$ (99%), Se powder (99%) and oleic acid (OA, 90%) were purchased from Aldrich. Oleylamine (OLA, $\geqslant$70%) was purchased from Fluka. Methanol, toluene, chloroform and acetone were obtained from commercial sources. All chemicals were used without further purification.

Synthesis of anisotropic shaped WZ-MnSe NCs

In a typical synthesis of tetrapod-shaped WZ-MnSe NCs, anhydrous $MnCl_2$ (0.032 g, 0.25 mmol), Se powder (0.02 g, 0.25 mmol), OA (4 mL) and OLA (4 mL) were added to a 50-mL three-necked flask. This mixture was heated to 200 °C for 4 h under a nitrogen flow, when the solution became a light orange colour. The solution was then heated to 300 °C at a rate of 2 °C min^{-1} and kept for 30 min under nitrogen flow. Then it was allowed to cool down to room temperature naturally. All samples were isolated using methanol and excess acetone and centrifuging for 10 min at 10 000 rpm and the products were collected. Comparative studies were investigated by changing the heating rates (15 and 25 °C min^{-1}) and volume ratio of the solvents (see below).

Characterization

Powder X-ray diffraction (XRD) data were collected on a Bruker D8 diffractometer working with a Cu-Kα target. Transmission electron microscope (TEM) images and selected area electron diffraction (SAED) patterns were obtained with a Hitachi H-8100 transmission electron microscope operating at an acceleration voltage of 200 kV. High-resolution TEM (HRTEM) images were obtained on a JEM-2100F operated at 200 kV, where the corresponding fast-Fourier transform (FFT) algorithms were analyzed. Absorption and PL spectra were measured by a Shimadzu UV-3150 spectrometer and a Photon Technology International photoluminescence instrument, respectively. Magnetic measurements were carried out by a Quantum Design MPMS SQUID VSM magnetometer. Quantification of WZ : ZB phase fractions was performed by using the *GSAS+EXPGUI* programs.[25]

Results and discussion

For the formation of different anisotropic shaped WZ-MnSe NCs by controlling heating rates, oleic acid (OA) and oleyl amine (OLA) were employed as the ligand and reaction solvent, as schematically shown in Fig. 1a. The shape and size of the produced MnSe NCs were characterized by transmission electron microscopy (TEM). As shown from the TEM images in Fig. 1b–d, the different heating rates resulted in the formation of different anisotropic shaped WZ-MnSe NCs. Fig. 1b shows a typical TEM image of the tetrapod-shaped MnSe NCs synthesized at a heating rate of 2 °C min^{-1}. The products have a relatively high yield (>90% of the obtained product consists of tetrapods; along with a few nanorods) (Fig. S1, ESI†). The length and diameter of the arms of the tetrapods are ~148 nm and ~30 nm, respectively. At a heating rate of 15 °C min^{-1}, monodisperse small waterdrop-shaped MnSe NCs with relatively uniform size were obtained in the reaction of tetrapod-shaped MnSe NCs (Fig. 1c). The length and diameter of the product are ~75 and ~40 nm, respectively. When the heating rate was increased to 25 °C min^{-1}, large waterdrop-shaped MnSe NCs were formed (~265 nm length, ~210 nm in diameter), as shown in Fig. 1d.

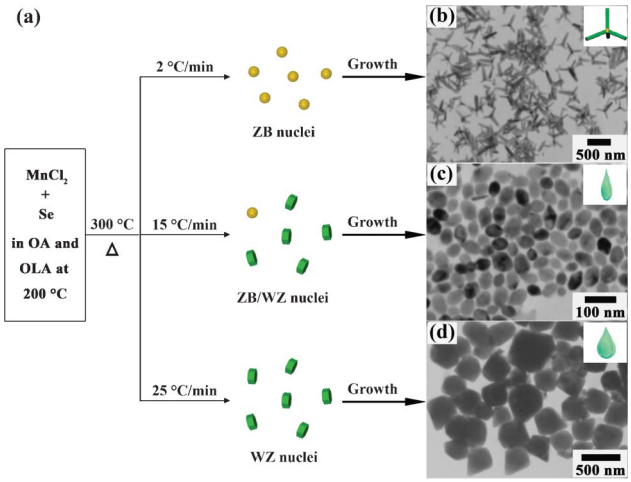

Fig. 1 (a) Schematic illustration of nucleation and growth process of anisotropic WZ-MnSe NCs at different heating rates. TEM images of (b) tetrapod-shaped MnSe NCs, (c) small waterdrop-shaped MnSe NCs and (d) large waterdrop-shaped MnSe NCs.

The crystal structure and chemical composition of the as-prepared samples were characterized by powder X-ray diffraction (XRD), as shown in Fig. 2a and b. All diffraction peaks correspond to hexagonal WZ-type MnSe.[17] The obvious diffraction peaks could be indexed to the (100), (002), (101), (102), (110), (103), (200), (112), (201) and (202) planes of hexagonal WZ MnSe. A selected area electron diffraction

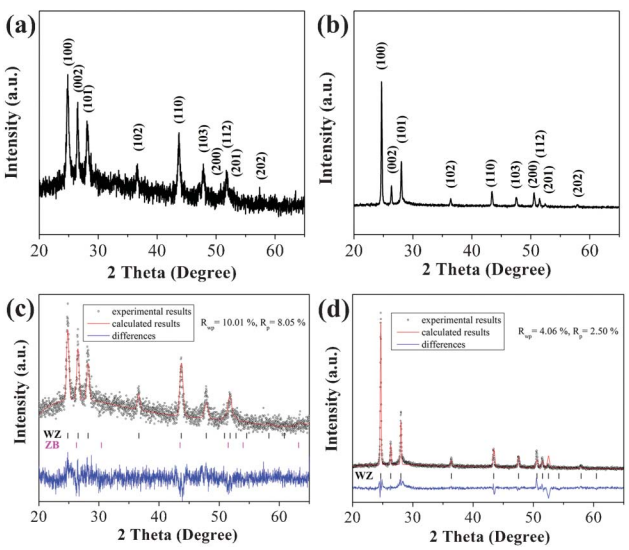

Fig. 2 XRD patterns and Rietveld refinement of the patterns: (a, c) tetrapod-shaped MnSe NCs; (b, d) large waterdrop-shaped MnSe NCs. The wavelength of XRD is 1.5406 Å.

(SAED) pattern of MnSe NCs is shown in Fig. S2 (ESI†). The diffraction rings in SAED correspond to the planes of the hexagonal WZ-type MnSe. The crystal structure of MnSe NCs from SAED agrees with that from XRD. It is known that the XRD peaks of ZB-MnSe (JCPDS 27-0311) overlap with that of WZ-MnSe and effectively add intensity to the (002), (110) and (112) peaks of WZ-MnSe. Hence, quantitative analysis of the XRD data indicates that the tetrapod-shaped MnSe NCs are composed of about 90% WZ-MnSe and 10% ZB polymorph (Fig. 2c). As shown in Fig. 2d, quantitative analysis of the XRD data indicates that the large waterdrop-shaped MnSe NCs are in pure hexagonal WZ structure.

The morphologies and crystal structures of WZ-MnSe NCs were further investigated by high-magnification TEM and high-resolution TEM (HRTEM). Fig. 3a presents a tetrapod-shaped MnSe NC with the outgoing arm nearly parallel to the electron beam. Four arms can be clearly observed if the sample is rotated to certain angles (Fig. 3a, inset). The four arms of the tetrapod are almost equal in length and diameter. The HRTEM image of a single arm shown in Fig. 3b exhibits that the fringe spacing is about 0.336 nm, corresponding to the (002) plane of WZ-MnSe. The fast-Fourier transform (FFT) pattern displayed in the inset shows that the arm has single-crystalline structure. HRTEM images of the waterdrop-shaped NCs also reveals (002) lattice fringes of crystalline WZ-MnSe (Fig. 3c and d). These results indicate that the growth direction of WZ-MnSe NCs is along the <001> direction. Furthermore, the heating rate also affected the overall aspect ratio of the WZ-MnSe NCs (Fig. S3, ESI†). It is known that a thermodynamically controlled condition (slow heating rate, 2 °C min^{-1}) generally enhances the growth rate along the *c*-axis in WZ crystal structure,[26,27] and thus generates anisotropic WZ-MnSe NCs with high aspect ratio (4.5 ± 0.6). At medium heating rate (15 °C min^{-1}), the aspect ratio drops down to 1.9 ± 0.2. In contrast, the kinetically controlled condition with rapid heating to 300 °C (25 °C min^{-1}) produces WZ-MnSe NCs with lowest aspect ratio (1.2 ± 0.1).

A solvothermal synthesis presents several advantages for synthesis and morphology control of uniform NCs. The crystalline face growth rates are respectively different, because the adsorption properties of surfactants on the particle surface differ according to the atomic arrangements. Simultaneously, the morphology of NCs is strongly influenced by the crystalline phase of nucleating seeds.[28] In general, the formation of NCs can be separated into two basic steps, nucleation and growth.[29,30] A schematic illustration of the nucleation and growth process of the MnSe NCs at different heating rates is shown in Fig. 1. In the present study, the heating rate plays the most important role in manipulating the final morphology. For the nucleation step, a slow heating rate results in more facile formation of the ZB-MnSe nucleus seeds, which are favored at low temperature. For the growth of group II–VI tetrapod-shaped NCs, Alivisatos and co-workers suggest that the tetrapod-shaped NC consists of a ZB core and four arms of WZ structure[31] and their model suggests that four WZ arms proceed evenly on the four different (111) planes of the ZB core using their WZ (001) planes. Because the two crystal planes have identical atomic structures no lattice mismatch will be introduced. In our previous work, we have observed the detailed formation processes of MnS nanobipods including ZB-core formation and WZ-arm growth.[32] Here, the formation processes of tetrapod-shaped MnSe NCs also have been investigated at different temperatures (Fig. S4, ESI†). According to the quantitative analysis of the XRD data, tetrapod-shaped MnSe NCs in our experiment are composed of ZB and WZ structures, and the HRTEM image shows that the arms are of single-crystalline WZ structure. So, it is suggested that the growth of tetrapod-shaped MnSe NCs follow the above-mentioned ZB-core–WZ-arm model.[33] At medium heating rate (15 °C min^{-1}), we also found a few tetrapod-shaped NCs, because a few ZB-MnSe nucleus seeds were formed in the early stage of nucleation (Fig. S5, ESI†). Therefore, a key factor in the formation of tetrapod morphology is that the ZB structure is adopted in the nucleation stage while the WZ structure is preferred during (anisotropic) crystal growth. With rapid heating, the WZ-nucleation seeds are favored over that of ZB-nucleation. The crystal structure has significant effects on the final crystal morphology. Since the growth rate along the *c*-axis is faster than those along other directions in the WZ structure, the nuclei gradually grow into tapering nanowaterdrops or other anisotropic shapes (such as nanorods, nanotears and nanotadpoles).[27,28] Also, different solvent systems were found to play important roles in obtaining various crystal structured nucleus seeds.[34] Modifying the volume ratio of the solvents could result

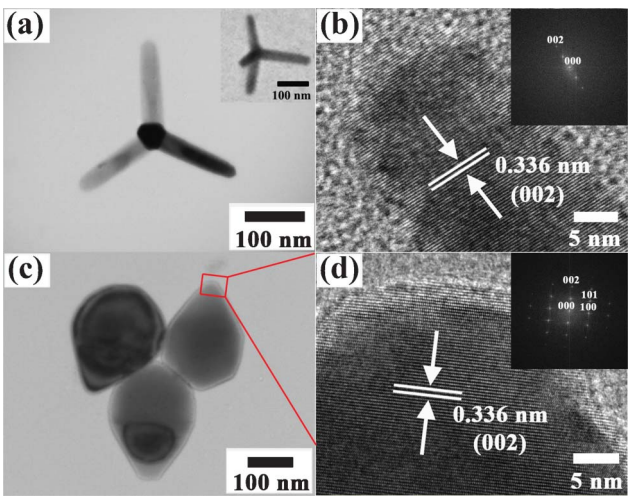

Fig. 3 High-magnification TEM (a, c) and HRTEM (b, d) images of the tetrapod- and waterdrop-shaped MnSe NCs. The insets of (a, b, d) show TEM images of a MnSe nanotetrapod and corresponding FFT patterns.

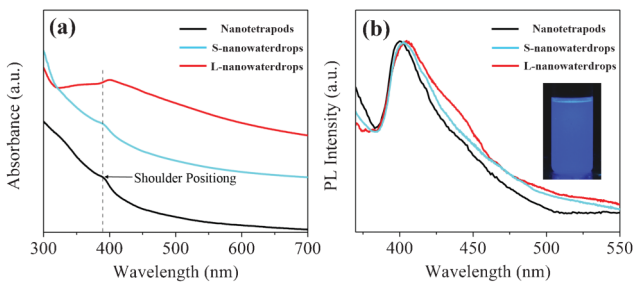

Fig. 4 Optical properties of the WZ-MnSe nanotetrapods, small (S) and large (L) nanowaterdrops: (a) UV-Vis absorbance spectra; (b) photoluminescence spectra (λ_{ex} = 350 nm). The inset of (b) shows a photograph of nanotetrapods under irradiation of a UV lamp.

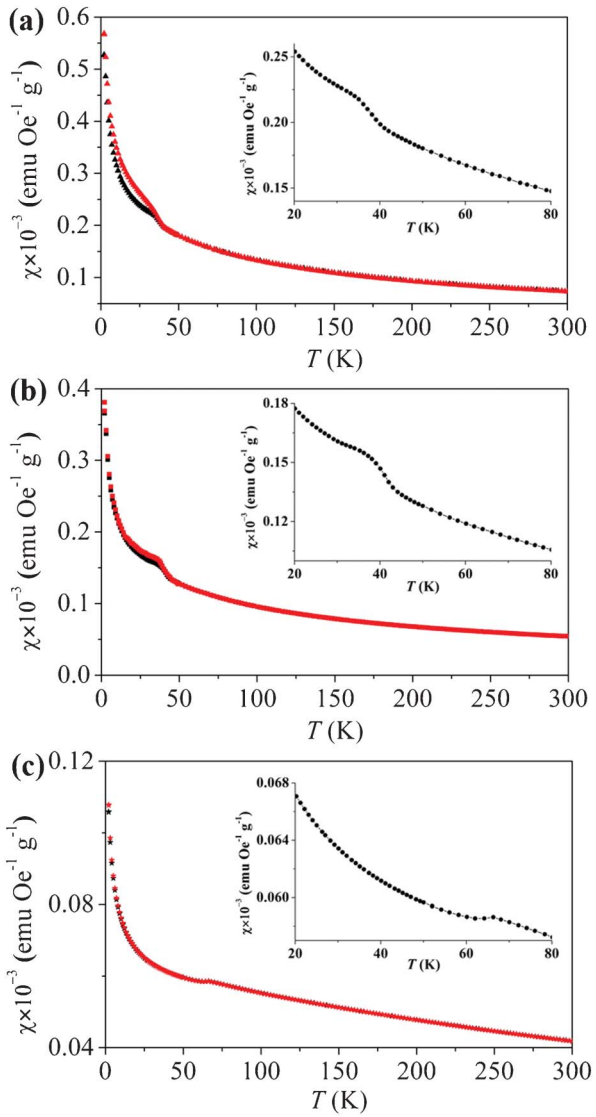

Fig. 5 FC (red) and ZFC (black) curves of (a) tetrapod-shaped MnSe NCs, (b) small waterdrop-shaped MnSe NCs and (c) large waterdrop-shaped MnSe NCs; small peaks at around 35, 38 and 67 K, suggestive of antiferromagnetic ordering, are resolved in the inset for the nanotetrapods and nanowaterdrops, respectively.

in the predominant formation of RS-MnSe NCs. For example, RS-MnSe NCs were obtained at an OA : OLA volume ratio of 1 : 3 (Fig. S6, ESI†). This indicates that RS-MnSe nucleus seeds were formed in the early stage of nucleation because the relative chemical environment for the configuration of the nuclei was changed.[35]

The successful synthesis of anisotropic shaped WZ-MnSe NCs allows us to investigate their optical and magnetic properties. The UV-Vis absorbance and PL spectra of the as-prepared tetrapod- and waterdrop-shaped MnSe NCs dispersed in chloroform solution were measured at room temperature (Fig. 4). A discernible shoulder peak at 389 nm ($E_g \approx 3.2$ eV) was detected in the tetrapod-shaped MnSe NCs (Fig. 4a), which is assigned to the optical transition of the excitonic state. This value is consistent with the band gaps of comparable WZ-MnS ($E_g = 3.2$ eV),[15] but slightly smaller than that for WZ-MnSe nanoparticles ($E_g \approx 3.5$ eV) due to the increase of size.[17] The shoulder peaks of the waterdrop-shaped MnSe NCs are red-shifted to 391 and 398 nm in comparison with that of the nanotetrapods, which can be attributed to the increase in diameter and the resultant smaller band gap, respectively. In addition, the tail of the absorbance spectra in large waterdrop-shaped MnSe NCs gradually extends through the visible light range. The broadening of the peak width is considered to arise from the size dispersity of the resultant waterdrop-shaped MnSe NCs. Fig. 4b shows the room-temperature PL spectra of these WZ-MnSe NCs within the range 400−405 nm, which exhibit blue–violet emission. These new architectures may be useful for full-colour displays and short wavelength optoelectronic devices.

The temperature dependence of magnetization measured in an applied field of 1000 Oe, clearly sheds light on the magnetic properties of these anisotropic WZ-MnSe NCs (Fig. 5). From the zero-field-cooled (ZFC) and field-cooled (FC) curves, it can be seen that the magnetization measurements show paramagnetic behaviour, which indicates that most of the Mn moments do not show ordered behavior.[17] For the tetrapod-shaped MnSe NCs, a small peak is clearly resolved at 35 K in the ZFC magnetization curve (Fig. 5a). It is suggested that some of the Mn moments have antiferromagnetic order with $T_N = 35$ K. This Néel temperature is close to that for WZ-MnS nanowires ($T_N = 30$ K),[15] but is smaller than for WZ-MnSe nanoparticles ($T_N = 64$ K).[17] In comparison, the ZFC curves exhibit higher Néel temperatures of 38 and 67 K for small and large waterdrop-shaped MnSe NCs, respectively (Fig. 5b and c). Our magnetization measurements for the WZ-MnSe NCs indicate that there is a mixture of antiferromagnetic and paramagnetic phases in the samples. Different from the isotropic WZ-MnSe nanoparticles, the transition temperature is

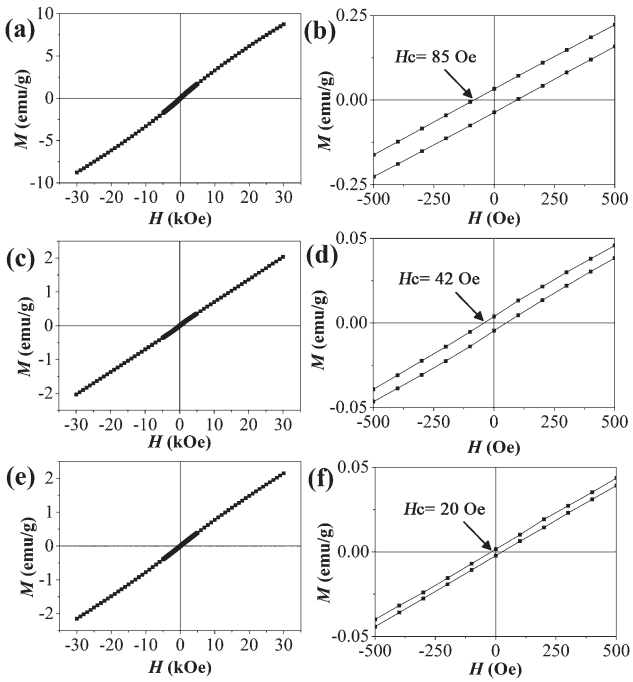

Fig. 6 Hysteresis loops of the WZ-MnSe NCs: (a) tetrapod-shaped MnSe NCs; (c) small waterdrop-shaped MnSe NCs; (e) large waterdrop-shaped MnSe NCs; (b), (d) and (f) show the region around zero fields, respectively.

reduced with decreasing diameter (Fig. S7, ESI†). Such a size-dependent phase-transition character has been demonstrated in ZB-MnSe films, RS-MnS and MnO NCs.[36–38] The size-dependent phase-transition behavior is attributed to a surface effect, because the anisotropic WZ-MnSe NCs have a larger surface area than the isotropic nanoparticles, and the Mn state at the surface is different from that inside a NC. The surface effect is strong enough to destroy the antiferromagnetic exchange coupling above the Néel temperature. The presence of a surface effect is further supported by the hysteresis measured at 5 K and 30 KOe, as shown in Fig. 6. It can be seen that the coercive force increases from 20 to 85 Oe with the increase of shape anisotropy. The loops indicate that the samples have weak ferromagnetism, which has been found in nanostructured antiferromagnetic materials as a result of the surface spins.[39,40] A core–shell structural model was proposed by Du *et al.*,[41] where relaxation of interaction on the surface of anisotropic NCs (nanorods or nanowires) allows the formation of a ferromagnetic shell, and the result is the generation of natural antiferromagnetic/ferromagnetic interfaces.[42] These results provide clear evidence for the existence of a surface effect in the anisotropic shaped WZ-MnSe NCs at low temperature.

Conclusions

In summary, we have reported a facile synthesis of anisotropic WZ-MnSe nanotetrapods by a one-pot solvothermal method. The morphology of MnSe NCs can be easily controlled to monodisperse nanowaterdrops with pure WZ structure by tuning the heating rate. Furthermore, these new architectures exhibit blue–violet photoluminescence, which may be used for full-colour displays and short wavelength optoelectronic devices. The magnetic measurements indicate that Néel temperature is reduced with decreasing nanocrystal diameter. The ability to control the shape and size of metastable NCs by tuning heating rates provides opportunities for creating novel devices, and also could be extended to the synthesis of other kinds of magnetic semiconductors with various anisotropic shapes.

Acknowledgements

This work is supported by NSFC (Nos. 21073071, 51102108, 51025206), the National Basic Research Program of China (No. 2011CB808200), Changjiang Scholar and Innovative Research Team in University (No. IRT1132), and Project 20121056 Supported by Graduate Innovation Fund of Jilin University.

References

1 C. B. Murray, D. J. Norris and M. G. Bawendi, *J. Am. Chem. Soc.*, 1993, **115**, 8706–8715.
2 J. S. Hu, L. L. Ren, Y. G. Guo, H. P. Liang, A. M. Cao, L. J. Wan and C. L. Bai, *Angew. Chem., Int. Ed.*, 2005, **44**, 1269–1273.
3 N. Pinna, K. Weiss, J. Urban and M. P. Pileni, *Adv. Mater.*, 2001, **13**, 261–264.
4 P. Leidinger, R. Popescu, D. Gerthsen, H. Lünsdorf and C. Feldmann, *Nanoscale*, 2011, **3**, 2544–2551.
5 Y. N. Wang, Q. Q. Dai, X. Y. Yang, B. Zou, D. M. Li, B. B. Liu, M. Z. Hu and G. T. Zou, *CrystEngComm*, 2011, **13**, 199–203.
6 R. E. Algra, M. Hocevar, M. A. Verheijen, I. Zardo, G. G. W. Immink, W. J. P. V. Enckevort, G. Abstreiter, L. P. Kouwenhoven, E. Vlieg and E. P. A. M. Bakkers, *Nano Lett.*, 2011, **11**, 1690–1694.
7 S. S. Warule, N. S. Chaudhari, B. B. Kale and M. A. More, *CrystEngComm*, 2009, **11**, 2776–2783.
8 G. J. Xiao, Q. F. Dong, Y. N. Wang, Y. M. Sui, J. J. Ning, Z. Y. Liu, W. J. Tian, B. B. Liu, G. T. Zou and B. Zou, *RSC Adv.*, 2012, **2**, 234–240.
9 W. Y. Kim, Y. C. Choi and K. S. Kim, *J. Mater. Chem.*, 2008, **18**, 4510–4521.
10 N. Pinna, G. Neri, M. Antonietti and M. Niederberger, *Angew. Chem., Int. Ed.*, 2004, **43**, 4345–4349.
11 A. Fiore, R. Mastria, M. G. Lupo, G. Lanzani, C. Giannini, E. Carlino, G. Morello, M. D. Giorgi, Y. Q. Li, R. Cingolani and L. Manna, *J. Am. Chem. Soc.*, 2009, **131**, 2274–2282.
12 M. D. Goodman, L. Zhao, K. A. DeRocher, J. Wang, S. K. Mallapragada and Z. Q. Lin, *ACS Nano*, 2010, **4**, 2043–2050.
13 S. Jun, S. H. Joo, R. Ryoo, M. Kruk, M. Jaroniec, Z. Liu, T. Ohsuna and O. Terasaki, *J. Am. Chem. Soc.*, 2000, **122**, 10712–10713.
14 J. Zhang, Q. Xu, Z. C. Feng, M. J. Li and C. Li, *Angew. Chem., Int. Ed.*, 2008, **47**, 1766–1769.
15 Y. W. Jun, Y. Y. Jung and J. Cheon, *J. Am. Chem. Soc.*, 2002, **124**, 615–619.
16 A. Gurlo, *Angew. Chem., Int. Ed.*, 2010, **49**, 5610–5612.
17 I. T. Sines, R. Misra, P. Schiffer and R. E. Schaak, *Angew. Chem., Int. Ed.*, 2010, **49**, 4638–4640.
18 T. M. Giebultowicz, N. Samarth, H. Luo, J. K. Furdyna, P. Klosowski and J. J. Rhyne, *Phys. Rev. B: Condens. Matter*, 1992, **46**, 12076–12079.
19 N. Samarth, P. Klosowski, H. Luo, G. Geibultowicz, J. K. Furdyna, J. J. Rhyne, B. E. Larson and N. Otsuka, *Phys. Rev. B: Condens. Matter*, 1991, **44**, 4701–4704.
20 W. Heimbrodt, O. Goede, I. Tschentsher and V. Weinhold, *Phys. B*, 1993, **185**, 357–361.
21 P. Tomasini, A. Haidoux, J. C. Tedenac and M. J. Maurin, *J. Cryst. Growth*, 1998, **193**, 572–576.
22 D. Litvinov, D. Gerthsen, A. Rosenauer, B. Daniel and M. Hetterich, *Appl. Phys. Lett.*, 2004, **85**, 751–753.
23 R. M. Murray, B. C. Forbes and R. D. Heyding, *Can. J. Chem.*, 1972, **50**, 4059–4061.
24 J. K. Furdyna, *J. Appl. Phys.*, 1988, **64**, R29–R64.
25 B. H. Toby, *J. Appl. Crystallogr.*, 2001, **34**, 210–213.
26 K. An, N. Lee, J. Park, S. C. Kim, Y. Hwang, J. G. Park, J. Y. Kim, J. H. Park, M. J. Han, J. Yu and T. Hyeon, *J. Am. Chem. Soc.*, 2006, **128**, 9753–9760.
27 K. M. Nam, J. H. Shim, D. W. Han, H. S. Kwon, Y. M. Kang, Y. Li, H. Song, W. S. Seo and J. T. Park, *Chem. Mater.*, 2010, **22**, 4446–4454.
28 M. Uehara, S. Sasaki, Y. Nakamura, C. G. Lee, K. Watanabe, H. Nakamura and H. Maeda, *CrystEngComm*, 2011, **13**, 2973–2983.
29 Y. D. Jin, X. F. Kang, Y. H. Song, B. L. Zhang, G. J. Cheng and S. J. Dong, *Anal. Chem.*, 2001, **73**, 2843–2849.
30 Z. A. Peng and X. G. Peng, *J. Am. Chem. Soc.*, 2001, **123**, 1389–1395.
31 L. Manna, D. J. Milliron, A. Meisel, E. C. Scher and A. P. Alivisatos, *Nat. Mater.*, 2003, **2**, 382–385.
32 X. Y. Yang, Y. N. Wang, K. Wang, Y. M. Sui, M. G. Zhang, B. Li, Y. M. Ma, B. B. Liu, G. T. Zou and B. Zou, *J. Phys. Chem. C*, 2012, **116**, 3292–3297.
33 M. Zhang, T. Y. Zhai, X. Wang, Y. Ma and J. N. Yao, *Cryst. Growth Des.*, 2010, **10**, 1201–1206.
34 G. Garnweitner and M. Niederberger, *J. Mater. Chem.*, 2008, **18**, 1171–1182.
35 Y. J. Zhang, H. R. Xu and Q. B. Wang, *Chem. Commun.*, 2010, **46**, 8941–8943.
36 N. Samarth, P. Klosowski, H. Luo, G. Geibultowicz, J. K. Furdyna, J. J. Rhyne, B. E. Larson and N. Otsuka, *Phys. Rev. B: Condens. Matter*, 1991, **44**, 4701–4704.
37 A. Puglisi, S. Mondini, S. Cenedese, A. M. Ferretti, N. Santo and A. Ponti, *Chem. Mater.*, 2010, **22**, 2804–2813.
38 S. H. Kan, I. Felner and U. Banin, *Isr. J. Chem.*, 2001, **41**, 55–62.
39 R. H. Kodama, S. A. Makhlouf and A. E. Berkowitz, *Phys. Rev. Lett.*, 1997, **79**, 1393–1396.
40 Q. W. Tian, M. H. Tang, F. R. Jiang, Y. W. Liu, J. H. Wu, R. J. Zou, Y. G. Sun, Z. G. Chen, R. W. Li and J. Q. Hu, *Chem. Commun.*, 2011, **47**, 8100–8102.
41 F. Du, Z. F. Huang, C. Z. Wang, X. Meng and G. Chen, *J. Appl. Phys.*, 2007, **102**, 113906.
42 M. H. Xu, W. Zhong, J. Y. Yu, W. C. Zang, C. Au, Z. X. Yang, L. Y. Lv and Y. W. Du, *J. Phys. Chem. C*, 2010, **114**, 16143–16147.

